Electronic Supplementary Material (ESI) for Chemical Science.

Table of Contents

S1. General Experimental Remarks

Powder X-Ray Diffraction (PXRD): PXRD patterns were collected in a PANalytical X'Pert PRO diffractometer using copper radiation (Cu Kα = 1.5418 Å) with an X'Celerator detector, operating at 40 mA and 45 kV. Profiles were collected in the 3° < 2θ < 40° range with a step size of 0.017°.

High angular resolution experiments of Synchrotron XRD were performed on the powder diffraction endstation of the MSPD beamline at the ALBA Synchrotron in Barcelona. [1]

The SXRD patterns were collected in the high-resolution multianalyzer detector (MAD) set-up with 13 keV beam energy (λ = 0.9531 Å). The samples were contained in quartz capillaries of 0.7 mm diameter, which were rotating during collection time.

Thermogravimetric Analysis (TGA): were carried out with a Mettler Toledo TGA/SDTA 851 apparatus between 25 and 800 °C under ambient conditions (10 °C·min−1 scan rate and an air flow of 9 mL·min−1).

Nuclear Magnetic Resonance Spectroscopy (NMR): NMR spectra were recorded on a Bruker AVIII 300 MHz spectrometer and referenced to residual solvent peaks.

Gas Uptake: N_2 adsorption isotherms were carried out at 77 K on a with a Micromeritics 3Flex gas sorption analyser. Samples were degassed under vacuum at 120 °C for 24 h in a Multisorb station prior to analysis. BET surface areas, micropore surface areas and external surface areas were calculated from the isotherms using the MicroActive operating software. The pore size distributions were calculated using Cylindrical pore oxide surface (QSDT) pore model within the MicroActive software, with no regularisation.

Scanning Electron Microscopy (SEM) and single point energy-dispersive X-Ray analysis (EDX): particle morphologies, dimensions and mapping were studied with a Hitachi S-4800 scanning electron microscope at an accelerating voltage of 20 kV, with no metalisation of the samples.

Fourier Transform Infrared Spectroscopy: IR spectra of solids were collected using a Shimadzu Fourier Transform Infrared Spectrometer, FTIR-8400S, fitted with a Diamond ATR unit.

Inductively Coupled Plasma-Mass Spectrometry: Metal content analyses were carried on an Agilent ICP-MS 7900 apparatus.

Computational generation of structural models: We created the models of MUV-10 defective structures by using Materials Studio 2017 R2.[2] We started with the single-crystal structure available from the Cambridge Structural Database (1819267) for a pristine cell of MUV-10 (3 clusters and 8 linkers), and constructed a 2 × 2 × 2 supercell (24 clusters and 64 linkers). To introduce vacants, the desired clusters and phenyl groups were manually removed and H atoms were added to complete the structure with formate groups (HCOO-). No further energy minimization was carried out after defect introduction, as results, all the structes share the same cell parameters (see supporting material CIF files).

S.2. Materials and Synthesis

All reagents were obtained from commercial sources and were used without further purification.

General remarks

For all modulated syntheses a mixture of solvents (8.8 mL of AcOH per 38.4 mL of DMF / 18.64 % v/v) was prepared in function of the number of reactions to perform (47.2 mL per reaction in the high scale, 11.8 mL per reaction in the low scale). This pre-made solvent mixture was used to separately dissolve the different synthetic components as further explained during this section.

In all syntheses, the jars were placed in an oven at room temperature and heated to 120℃ with 2℃/min ramp. The temperature was maintained for 24 hours and cooled down to room temperature with 0.4℃/min ramp. The resultant powder was collected by centrifugation (5000 rpm, 5 min) and washed with DMF (X2) and MeOH (x3) through dispersion-centrifugation cycles. The samples were dried under vacuum overnight and further activated by soxhlet with MeOH during approximately 24 hours. The samples were further dried under vacuum for 24 hours prior to characterization.

Procedure for the exploration of the role of btc depletion in MUV-10 synthesis. In 50 mL pyrex jars, $CaCl_2$ (1 equivalent, 266 mg, 2.4mmol) was dissolved in 10 mL of solvent mixture. In a separate vial, btc (number of equivalents desired for each synthesis, tabulated in Table SX), was dissolved in 37.2 mL of solvent mixture. The $CaCl_2$ solution was added to the btc containing jar and the mixture was gently stirred, followed by slow Ti(IV) isopropoxide addition (1 equivalent compared to $CaCl_2$) and gentle stirring.

Table S1: Tabulated synthetic conditions of MUV-10 synthesised with depleted amount of btc. The samples labelling corresponds to the account of btc (equivalents compared to metal) added, in comparison to the amount needed to form a pristine structure, for which the ratio btc /Metal (Ti or Ca) is 1.33 (8 btc per 3 clusters in the unit cell, corresponding to 6 Ti and 6 Ca).

Sample	**$CaCl_2$**	**$Ti(O^iPr)_4$**	**btc**	**Volume**	**btc vs metal**	**btc Vs Pristine (L:M 1:1.33)**
	Mass/ mmol	**µL/ mmol**	**Mass/ mmol**	**DMF/ AcOH**	**Equivalents**	**%**
MUV-10 (H)	266 mg 2.4 mmol	710 µL 2.4 mmol	757 mg 3.6 mmol	38.4 mL 8.8 mL	1.5	112.78
MUV-10 (75% btc)	266 mg 2.4 mmol	710 µL 2.4 mmol	504 mg 2.4 mmol	38.4 mL 8.8 mL	1	75.19
MUV-10 (56% btc)	266mg 2.4 mmol	710 µL 2.4 mmol	307 mg 1.8 mmol	38.4 mL 8.8 mL	0.75	56.39
MUV-10 (38% btc)	266mg 2.4 mmol	710 µL 2.4 mmol	205 mg 1.2 mmol	38.4 mL 8.8 mL	0.5	37.59
MUV-10 (23% btc)	266mg 2.4 mmol	710 µL 2.4 mmol	122 mg 0.72 mmol	38.4 mL 8.8 mL	0.3	22.56

S.3 Effect of linker concentration in synthesised MUV-10 samples.

S.3.1 Scanning Electron Microscopy (SEM)

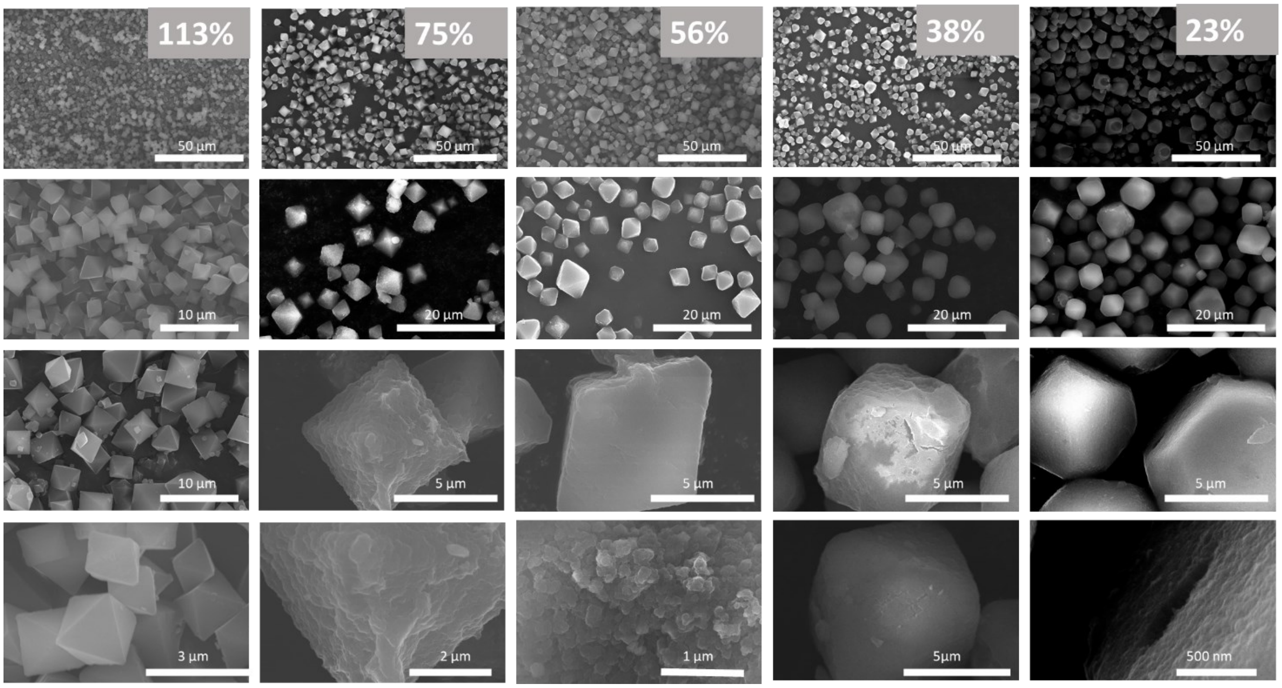

Figure S1: SEM images of MUV-10 synthesised with depleting amounts of btc, showing the formation of hierarchical crystals in which the nanoparticle size decrease with btc depletion.

Table S2: Tabulated particle sizes. standard deviations and metal content of MUV-10 synthesised under different conditions.

Sample	**Crystal´s size (SD) (nm)**	**NPs Size (SD) (nm)**
MUV-10 (113% btc)	3064 (1933)	n/a
MUV-10 (75% btc)	6071 (1390)	269 (73)
MUV-10 (56% btc)	6804 (1238)	149 (66)
MUV-10 (38% btc)	8244 (1786)	84 (32)
MUV-10 (23% btc)	10809 (1429)	41 (17)

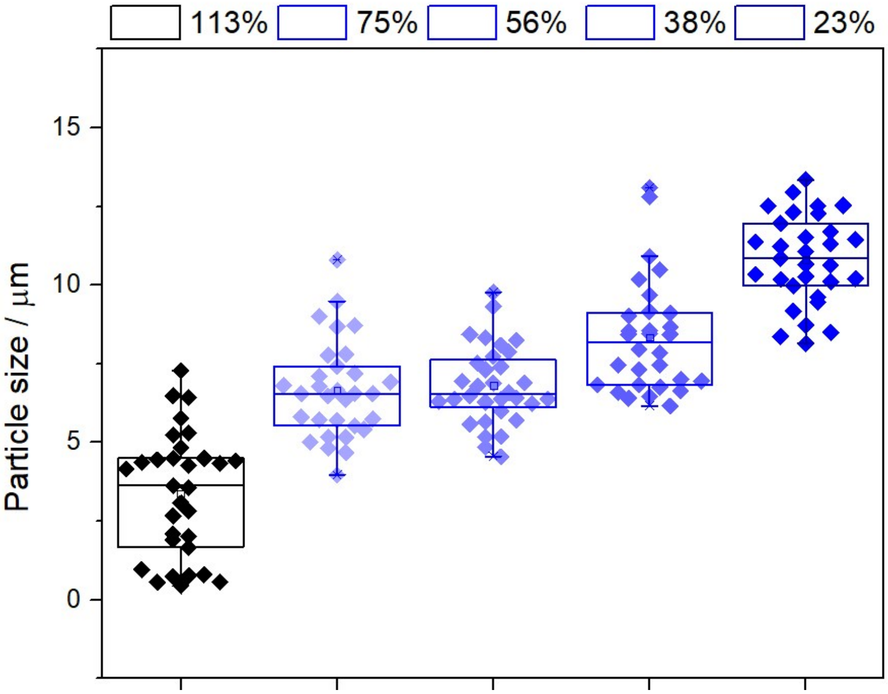

Figure S2: Histograms displaying particle size of MUV-10 depleting amounts of btc. Bin size 500 nm

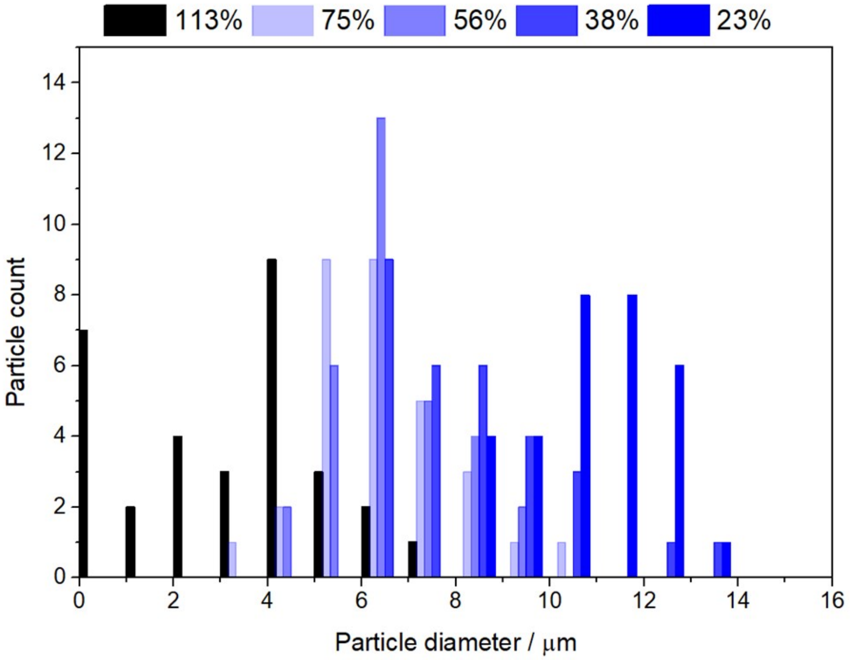

Figure S3: Histograms displaying hierarchical crystals size of MUV-10depleting amounts of btc. Bin size 1 μm

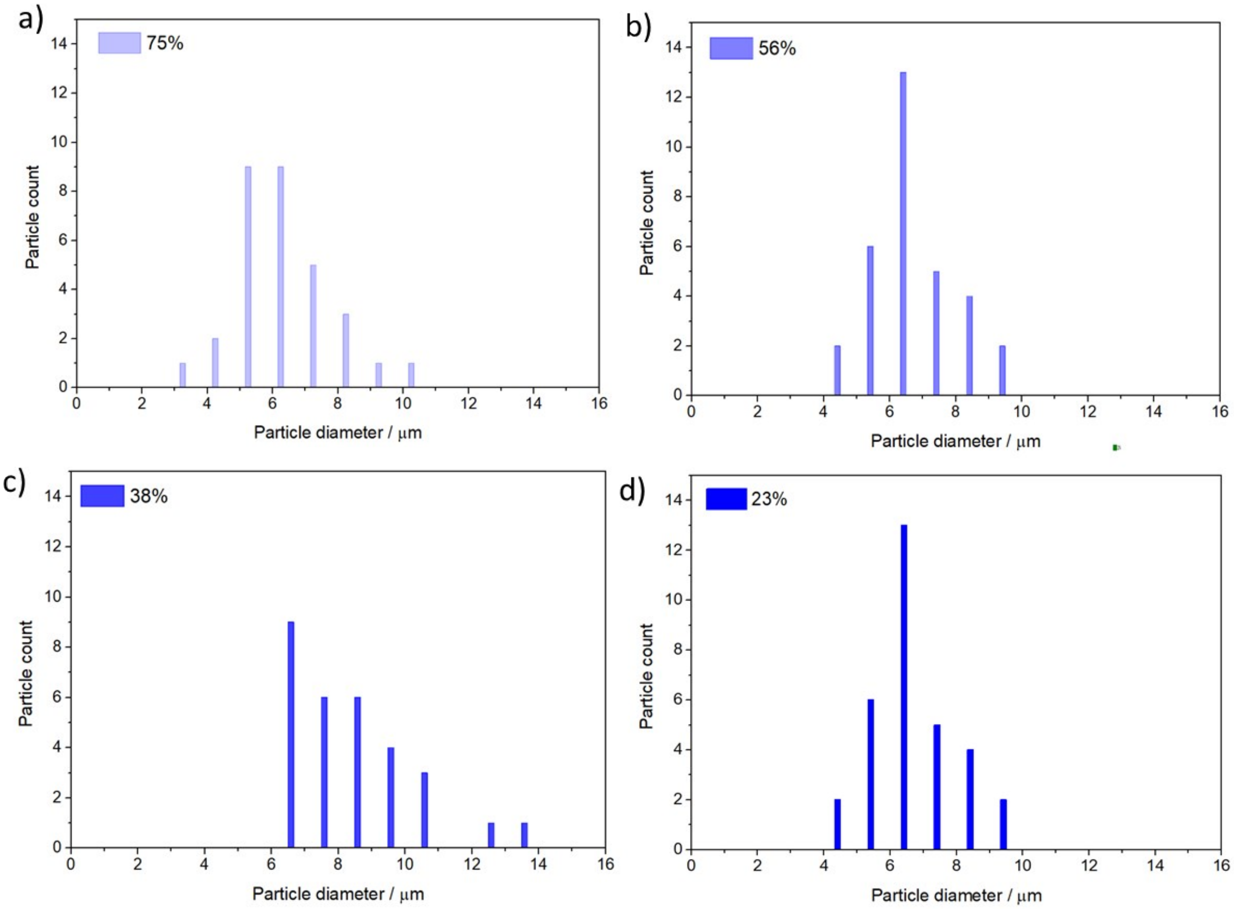

Figure S4: Histograms displaying hierarchical crystals size of MUV-10 depleting amounts of btc. Bin size 1 μm

S.3.2 Proton Nuclear Magnetic Resonance (^{1}HNMR)

Table S3: Tabulated values of the number of modulators per btc, calculated by ^{1}HNMR as (number modulator) / (number btc) after soxhlet activation, showing very small variation among three different batches.

Sample	AcOH/btc	SD	FA/btc	SD
MUV-10 (H)	0.000	0.000	0.015	0.001
MUV-10 (75% btc)	0.033	0.003	0.064	0.039
MUV-10 (56% btc)	0.120	0.000	0.088	0.040
MUV-10 (38% btc)	0.357	0.015	0.097	0.030
MUV-10 (23% btc)	0.991	0.027	0.115	0.027

Table S4: Tabulated values of the number of modulators per btc, calculated by ^{1}HNMR as (number modulator) / (number btc) of the high scale batch after soxhlet activation (used for further characterisation).

Sample	AcOH/btc	FA/btc	(AcOH + FA)/btc
MUV-10 (H)	0	0.015	0.015
MUV-10 (75% btc)	0.030	0.114	0.144
MUV-10 (56% btc)	0.120	0.137	0.257
MUV-10 (38% btc)	0.373	0.132	0.505
MUV-10 (23% btc)	0.965	0.145	1.110

Table S5: Tabulated values of the per cent of modulator compared to btc, calculated by ^{1}HNMR as (number modulator) / (number modulator + number btc)*100 of the high scale batch after soxhlet activation (used for further characterisation).

Sample	AcOH mol%	FA mol%	Total modulator mol%
MUV-10 (H)	0.000	1.503	1.503
MUV-10 (75% btc)	2.918	10.246	12.604
MUV-10 (56% btc)	10.713	12.039	20.436
MUV-10 (38% btc)	27.153	11.650	33.538
MUV-10 (23% btc)	49.104	12.642	52.595

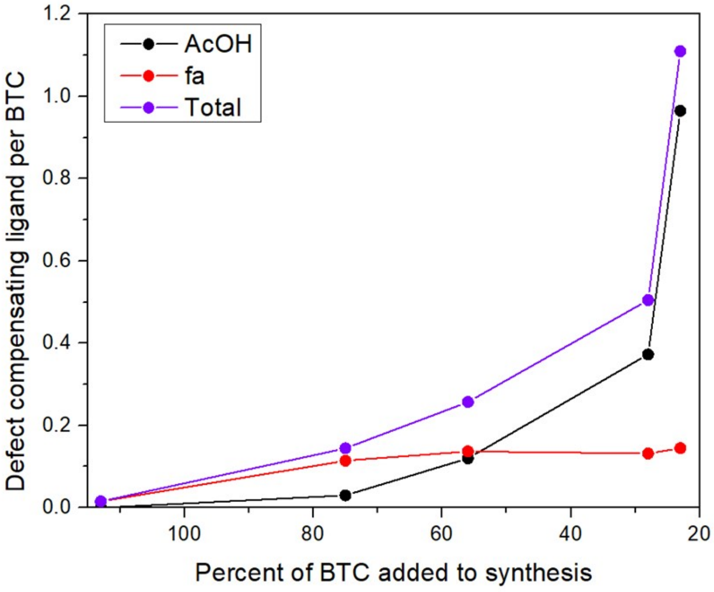

Figure S5: Representation of formic acid. acetic acid and total modulator (formic acid and acetic acid) per btc (molar ratio), determined ^{1}HNMR, as a function of the btc per cent of btc during synthesis in comparison with the amount of btc needed to form a defect-free structure, showing an increase in formic acid incorporation with btc depletion.

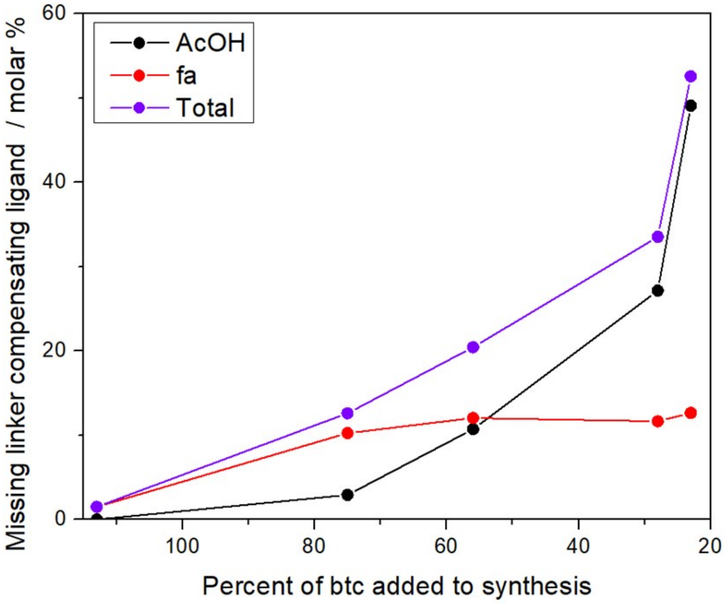

Figure S6: Representation of formic acid, acetic acid and total modulator (formic acid and acetic acid) per btc, determined in molar per cent by ^{1}HNMR, as a function of the btc per cent of btc during synthesis in comparison with the amount of btc needed to form a defect-free structure, showing an increase in formic acid incorporation with btc depletion.

S.3.3 Fourier Transformed Infrared spectroscopy (FT-IR)

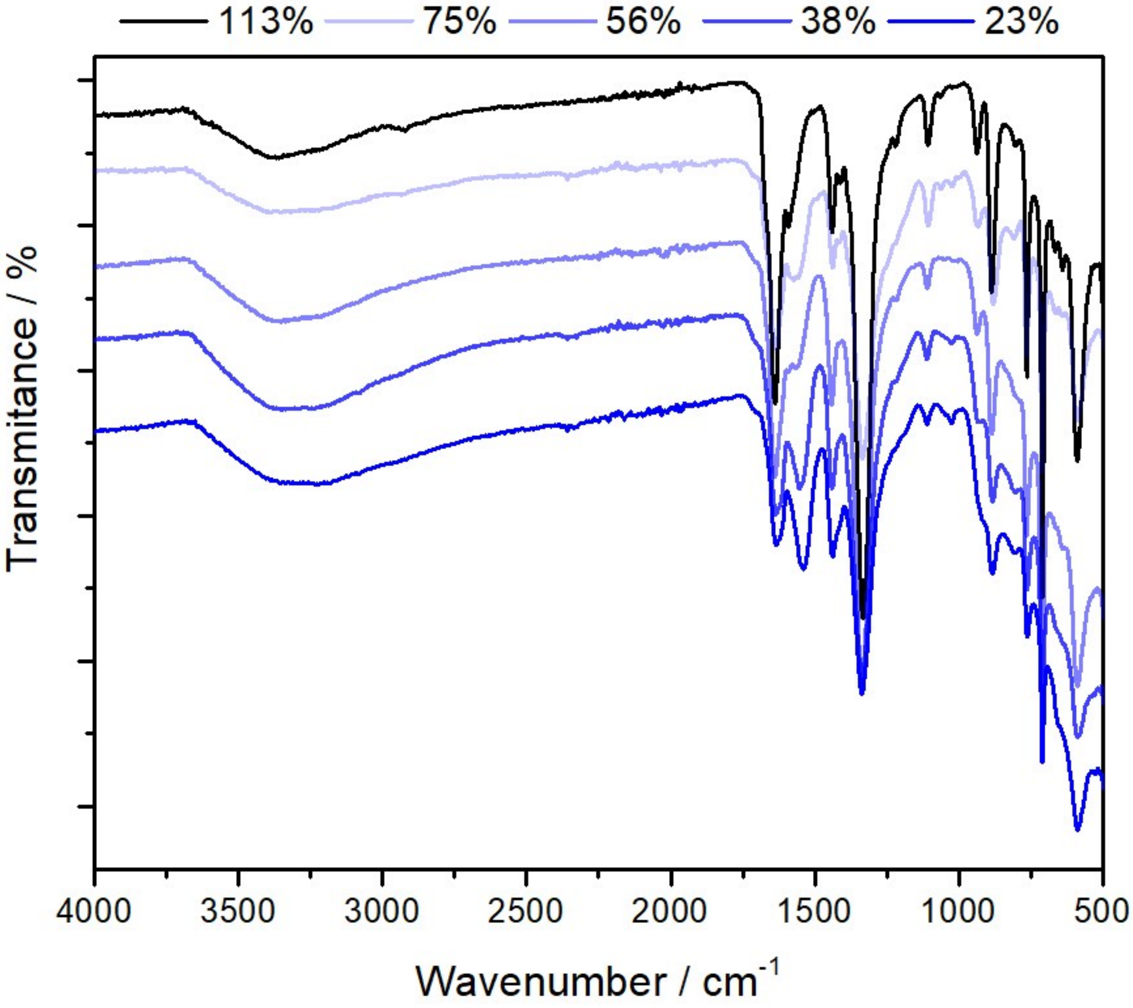

Figure S7: Raw FT-IR profiles of MUV-10 synthesised with depleting btc concentration compared to pristine MUV-10. Changes in the metal vibration bands at ca. 650 cm^{-1}, together with the broadening of the carboxylate signals, indicates defectivity upon incorporation of fa/AcOH.

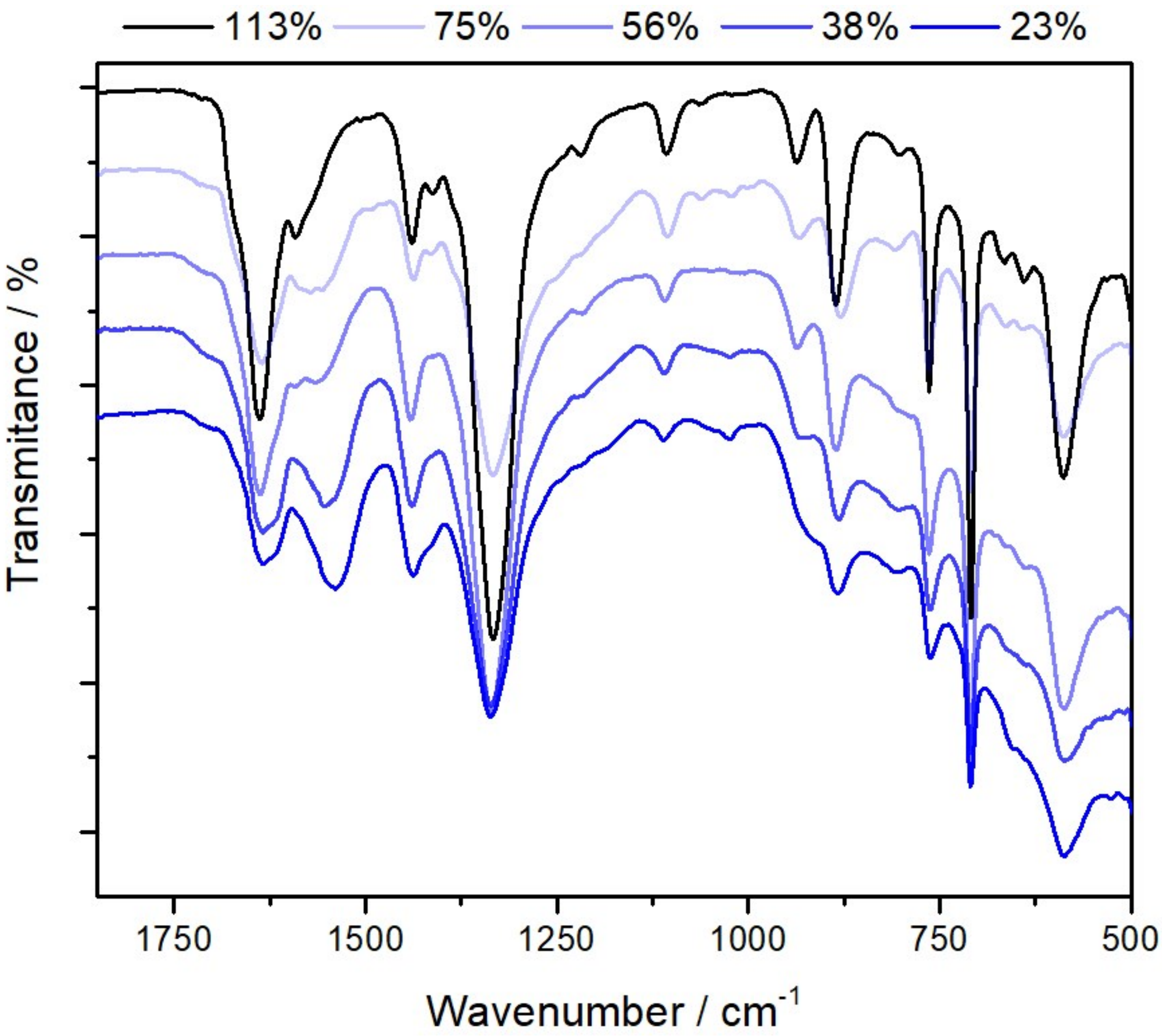

Figure S8: Raw FT-IR profiles of MUV-10 synthesised with depleting btc concentration compared to pristine MUV-10. Changes in the metal vibration bands at ca. 550 cm^{-1}, together with the broadening of the carboxylate signals, indicates defectivity. Characteristic bands of coordinated carboxylate anions can be observed: ca. 1536 cm^{-1} O-C-O sym/assym and ca. 1019 cm^{-1} COO-δ, which increases in intensity as btc is reduced, while no free carboxylate bands are observed, confirming modulators' attachment.

S.3.4 Thermogravimetric analysis (TGA)

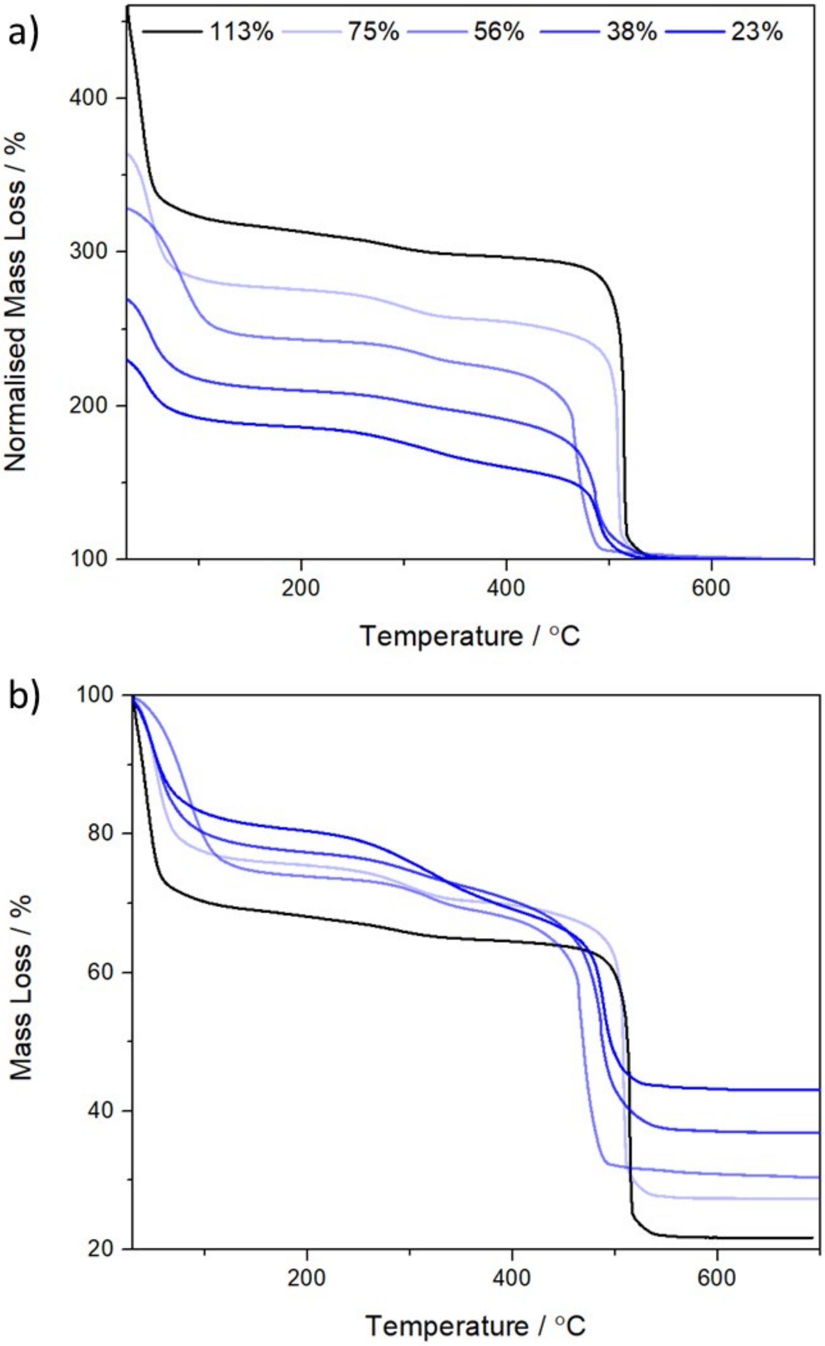

Figure S9: TGA profiles of MUV-10 synthesised with depleting btc, compared to pristine MUV-10. The btc decomposition step drastically decreases while the defect-compensating step at 200-400ºC increases, in great agreement with ^{1}HNMR showing a relation between btc depletion and the incorporation of formic acid and acetic acid.

Table S6: Data extracted from TGA analysis

Sample	Exp MS % 250ºC	Ms% (450ºC)
MUV-10 (H)	312	289
MUV-10 (75% btc)	283	248
MUV-10 (56% btc)	248	221
MUV-10 (38% btc)	219	184
MUV-10 (23% btc)	191	157

[3]**Table S7:** Data extracted from TGA analysis. Model structure: $[TiCaO(H_2O)_w(btc)_x(fa)_y(AcOH)_z(OH)_d]$ [3]

Sample	btc/Ti	FA /Ti	AcOH/Ti	OH/Ti	H_2O/Ti	ML%	Coordination positions
MUV-10 (H)	1.403	0.013	0.000	-0.222	1.6	-5.5	12.8
MUV-10 (75% btc)	1.099	0.118	0.044	0.542	2.0	17.4	12.5
MUV-10 (56% btc)	0.898	0.123	0.108	1.075	0.9	32.5	10.9
MUV-10 (38% btc)	0.624	0.082	0.232	1.815	0.9	53.1	10.1
MUV-10 (23% btc)	0.423	0.061	0.408	2.261	0.2	68.2	8.9

Table S8: Estimated composition of capping ligands.

Sample	**Estimated composition**
MUV-10 (H)	$TiCaO(H_2O)_{1.8}(btc)_{1.40}(FA)_{0.01}$
MUV-10 (75% btc)	$TiCaO(H_2O)_2(btc)_{1.10}(FA)_{0.12}(AcOH)_{0.04}(OH)_{0.54}$
MUV-10 (56% btc)	$TiCaO(H_2O)_{0.9}(btc)_{0.90}(FA)_{0.12}(AcOH)_{0.11}(OH)_{1.1}$
MUV-10 (38% btc)	$TiCaO(H_2O)_{0.9}(btc)_{0.62}(FA)_{0.08}(AcOH)_{0.27}(OH)_{1.82}$
MUV-10 (23% btc)	$TiCaO(H_2O)_{0.2}(btc)_{0.42}(FA)_{0.06}(AcOH)_{0.41}(OH)_{2.26}$

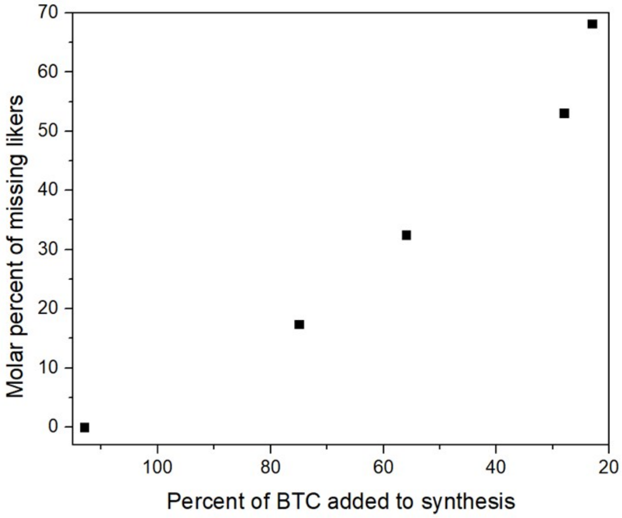

Figure S10: Experimental molar per cent of missing linkers calculated by TGA as a function of the per cent of btc added to synthesis.

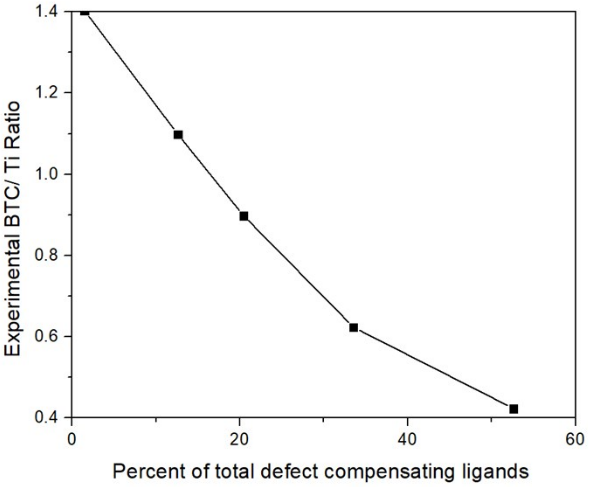

Figure S11: Experimental btc/metal ratio calculated by TGA as a function of the per cent of modulator (FA and AcOH) molecules versus the total amount of linker (btc) and ligands (fa and AcOH), determined by ^{1}HNMR ($R^2 = 0.9798$). This suggests that the amount of btc is directly related to the amount of total defect commentating ligands in comparison with btc. Hence, defect ligands much be attached through the MOF structure and not at the surface.

S.3.5 Metal content

Table S9: Tabulated values of molar per cent of Ca and Ti calculated for 3 different batches by EDX.

Sample	EDX			
	% Ca	*SD Ca*	*% Ti*	*SD Ti*
MUV-10 (H)	46.37	0.33	53.63	0.33
MUV-10 (75% btc)	49.43	0.15	50.57	0.15
MUV-10 (56% btc)	40.76	1.73	59.24	1.73
MUV-10 (38% btc)	35.42	4.24	64.58	4.24
MUV-10 (23% btc)	38.67	1.57	61.33	1.57

S.3.6 N_2 gas isotherms.

Table S10: Tabulated data extracted from N_2 adsorption and desorption measurements of MUV-10 (Figure 2f in the manuscript) synthesised with different quantities of btc showing a decrease in microporosity with btc depletion, together with an increase in mesoporosity.

Sample	SA_{BET} / SA_{MICRO}/ SA_{EXT} (m^2/g)	Micro / Mesopore volume (cm^3/g)		Pore volume (cm^3/g)
MUV-10 (H)	1041/ 950 / 91	0.365	0.008	0.373
MUV-10 (75% btc)	871/ 713 /158	0.3124	0.104	0.416
MUV-10 (56% btc)	723 / 498 /225	0.244	0.161	0.405
MUV-10 (38% btc)	652 / 413 /240	0.202	0.187	0.389
MUV-10 (23% btc)	478/ 253 /225	0.127	0.151	0.278

The BET surface areas were calculated with the native analysis software available from the 3Flex gas sorption analyser (MicroActive version 4.02, e572371, Micromeritics). Fitting to the BET equation was performed semiautomatically by using at least 5 points in the interval $0.05 \leq P/P_0 \leq 0.30$ according to the Rouquerol criteria. We ensured positive values for C and y-intercept by manual selection in all cases. The micropore surface areas and micropore pore volumes were calculated using the t-plot with Harkins and Jura thickness curve based on the BET surface areas. The total pore volumes were calculated from the uptake of the isotherms at $P/P_0 =0.9$. The external surface areas were calculated as the substraction of the micropore surface areas to the BET areas, while the mesopore volumes were calculated by subtracting the micropore volumes to the total pore volumes.

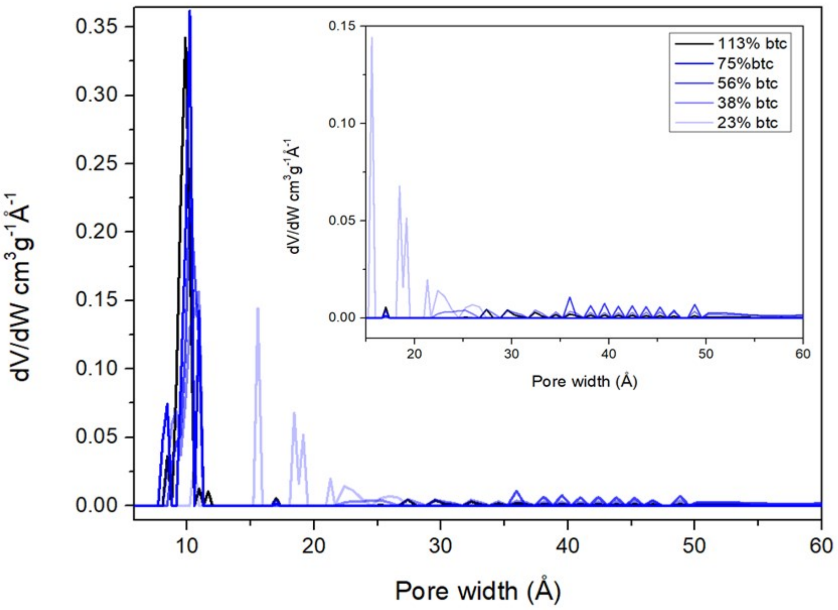

Figure S12: Pore size distributions extracted from the N_2 adsorption and desorption isotherms of MUV-10 synthesised with depleting BTC concentration. Pore size distributions calculated with NLSDFT Cylindrical oxide surface. No Regularisation.

S.4 Correlation of changes in porosity and diffraction in defective MUV-10 frameworks

S.4.1 Simulated pore size distribution (PSD).

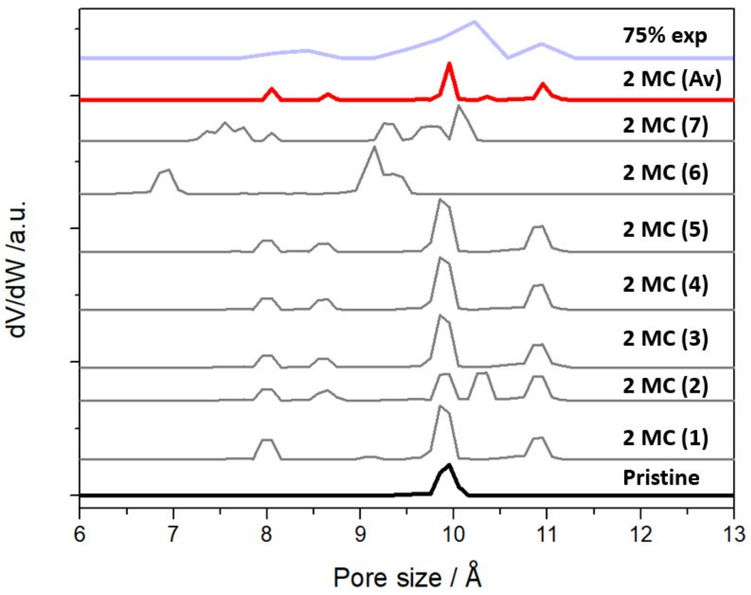

Figure S13: Experimental PSD of the 75% sample compared with the simulated PSDs of pristine MUV-10, the 7 possible MUV-10 model structures with 2 missing clusters in the 2x2x2 supercell and the average PSD of those structures. Pore size calculation for each structure was carried out using Zeo++[4] (chan_radious=probe_ratious=0.9 and num_samples=2000). Simulated data has been shifted by -1.6.

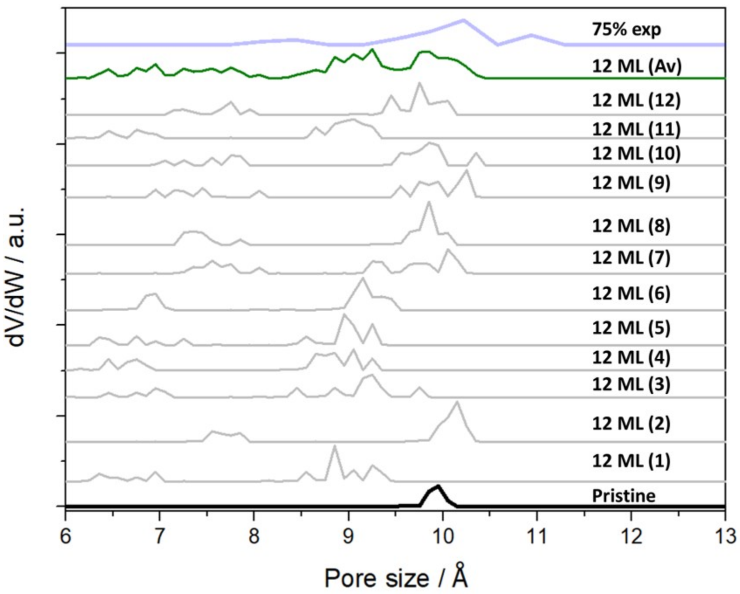

Figure S14: Comparison of the experimental PSD of the 75% sample with the simulated PSDs of pristine MUV-10, and configurations of MUV-10 with 12 missing linkers in the 2x2x2 supercell, according to the stoichiometry determined for 75% by TGA and NMR measurements, showing that the ML models do not correlate with the experimental PSD of 75%.

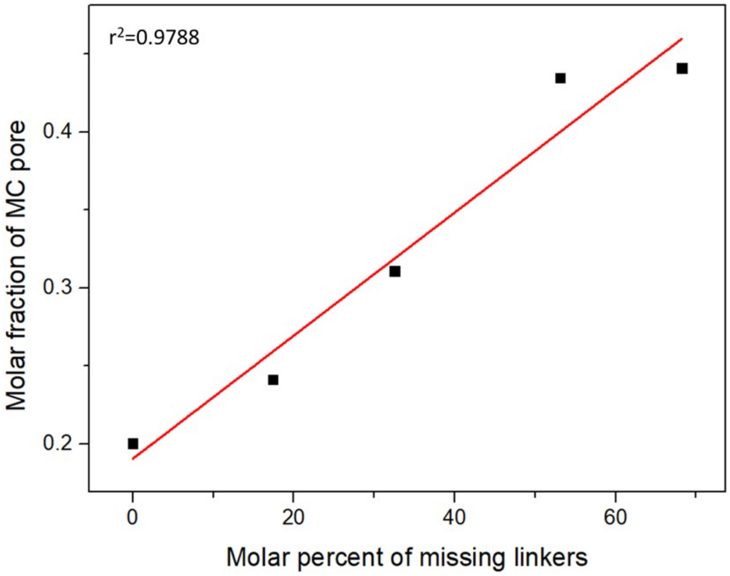

Figure S15: Linear relation between the molar per cent of missing linkers determined from TGA and the molar ratio of pore volume contribution from the missing cluster topology.

S.4.2 Simulated PXRD patterns.

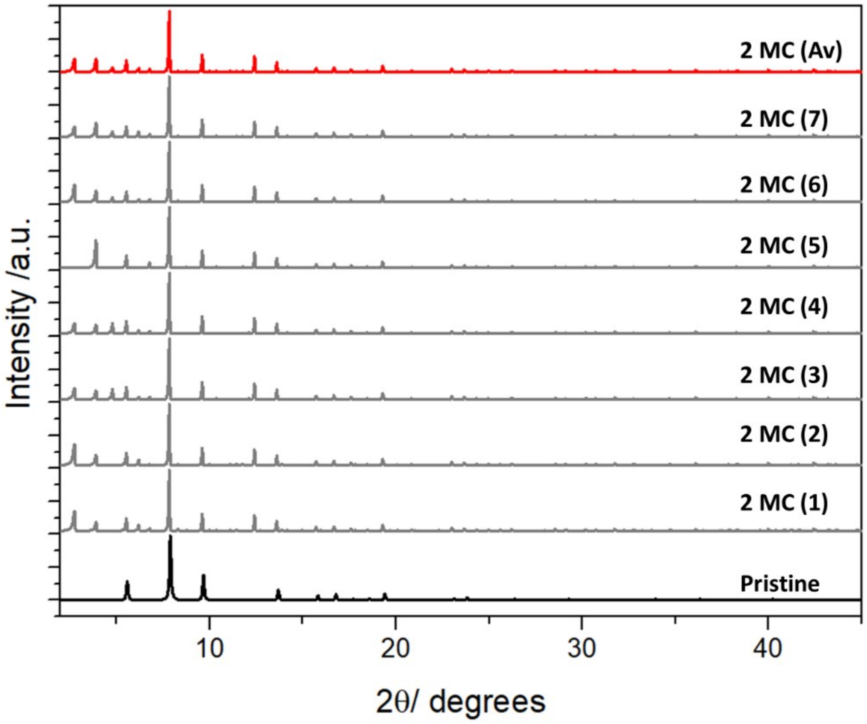

Figure S16: Simulated PXRD patterns of MUV-10 and MUV-10 with 2 missing clusters in a 2x2x2 unit cell.

Table S11. Simulated surface area of pristine and 2 missing clusters MUV-10 2 x 2 x 2 supercells. Surface area for each structure was determined using Zeo++[4] (chan_radious=probe_ratious=1.92 and num_samples=100000). Calculated total surface areas of 113% and 75% samples have been added for comparison.

	Pris.	**2MC (1)**	**2MC (2)**	**2MC (3)**	**2MC (4)**	**2MC (5)**	**2MC (6)**	**2MC (7)**	**2M (Av)**	**113%**	**75%**
SA (m^2/g)	1049	1457	1452	1457	1457	1457	1417	1457	1450	1041	871

Rereferences

1 F. Fauth, I. Peral, C. Popescu and M. Knapp, *Powder Diffr.*, 2013, **28**, 360–370.

2 M. Meunier, *Mol. Simulat.*, 2008, **34**, 887–888.

3 I. A. Lázaro, *Eur. J. Inorg. Chem.*, 2020, **2020**, 4284-4294.

4 R. L. Martin, B. Smit and M. Haranczyk, *J. Chem. Inf. Model.*, 2011, **52**, 308–318.